

Gradient-adaptive Nonlinear Sharpening for Dental Radiographs

Original Scientific Paper

Manoj T Joy

Sathyabama Institute of Science and Technology, Chennai, India
manojtjoy@gmail.com

B Priestly Shan

Chandigarh University, Punjab, India
priestlyshan@gmail.com

Geevarghese Titus

Amal Jyothi College of Engineering, Kanjirapally, Kerala, India
geevarghesetitus@amaljyothi.ac.in

Abstract – *Unsharp Masking is a popular image processing technique used for improving the sharpness of structures on dental radiographs. However, it produces overshoot artefact and intolerably amplifies noise. On radiographs, the overshoot artefact often resembles the indications of prosthesis misfit, pathosis, and pathological features associated with restorations. A noise-robust alternative to the Unsharp Masking algorithm, termed Gradient-adaptive Nonlinear Sharpening (GNS) which is free from overshoot and discontinuity artefacts, is proposed in this paper. In GNS, the product of the arbitrary scalar termed as 'scale' and the difference between the output of the Adaptive Edge Smoothing Filter (AESF) and the input image, weighted by the normalized gradient magnitude is added to the input image. AESF is a locally-adaptive 2D Gaussian smoothing kernel whose variance is directly proportional to the local value of the gradient magnitude. The dataset employed in this paper is downloaded from the Mendeley data repository having annotated panoramic dental radiographs of 116 patients. On 116 dental radiographs, the values of Saturation Evaluation Index (SEI), Sharpness of Ridges (SOR), Edge Model Based Contrast Metric (EMBCM), and Visual Information Fidelity (VIF) exhibited by the Unsharp Masking are 0.0048 ± 0.0021 , $4.4 \times 10^{13} \pm 3.8 \times 10^{13}$, 0.2634 ± 0.2732 and 0.9898 ± 0.0122 . The values of these quality metrics corresponding to the GNS are 0.0042 ± 0.0017 , $2.2 \times 10^{13} \pm 1.8 \times 10^{13}$, 0.5224 ± 0.1825 , and 1.0094 ± 0.0094 . GNS exhibited lower values of SEI and SOR and higher values of EMCBM and VIF, compared to the Unsharp Masking. Lower values of SEI and SOR, respectively indicate that GNS is free from overshoot artefact and saturation and the quality of edges in the output images of GNS is less affected by noise. Higher values of EMCBM and VIF, respectively confirm that GNS is free from haloes as it produces thin and sharp edges and the sharpened images are of good information fidelity.*

Keywords: Dental radiograph; Dental X-ray images; Image sharpening; Overshoot artefact; Unsharp Masking

1. INTRODUCTION

1.1. BACKGROUND & PROBLEM DOMAIN

The advent of advanced image processing algorithms and machine learning techniques has revolutionized the automated analysis of dental radiographs. Many recent methods make use of image processing algorithms and machine learning techniques for the diagnosis of Periodontal Bone Loss (PBL) [1, 2], Osteoporosis [3, 4], and dental caries [5] from dental radiographs. Apart from the clinical applications, dental radiographs are used for the automated identification

of humans in forensic odontology [6]. The majority of these methods used in clinical practice and forensic odontology involve the segmentation of structures like teeth and mandibles from the dental radiograph [7, 8].

Segmentation of structures from the dental radiograph is often difficult as the structures in it may not have sharp boundaries. The lack of sharpness could be due to the factors like inappropriate positioning, over-exposure, movement of patient/equipment during exposure, etc. Powerful post-processing algorithms are required to improve the sharpness of edges and to improve the accuracy of the segmentation of structures from dental radiographs.

1.2. REVIEW OF LITERATURE

Post-processing algorithms available in literature meant for improving the quality of dental radiographs can be classified into three categories. These categories are denoising, contrast enhancement, and sharpening algorithms. The denoising algorithms include a 2-D Butterworth low-pass filter (frequency domain) [9], Bayesian Least Squares - Gaussian Scaled Mixture (BLS-GSM) algorithm, and Total Variation (TV) filter [10]. Contrast Limited Adaptive Histogram Equalization (CLAHE) [11, 12] is an algorithm in literature meant for improving the contrast in dental radiographs. Unsharp Masking is the most popular algorithm used for improving the sharpness of dental radiographs. Yan et al. [13] proposed Bi-SCM: bidirectional spiking cortical model an adaptive unsharp mask using a bio-inspired neural network. To improve the x-ray, Skewness Reformed Complex Diffusion (SRCD) is proposed in [14] where the skewness of the images is used as a parameter to configure the smoothing filtering of the unsharp mask.

Many decades before itself, Fujita *et al.* [15] had demonstrated the prospect of Unsharp Masking for enhancing the quality of dentomaxillofacial radiographs. Harada *et al.* [16] used Unsharp Masking for sharpening the bony structure in the maxillofacial region in the three-dimensional Computed Tomography (CT) image. Couture *et al.* [17] used Unsharp Masking to enhance the texture of cortical and trabecular bones on the projection radiographs of mandibles to effectively visualize the high-frequency variations in bone mineral density. Recently, Geraets *et al.* [18] used Unsharp Masking to enhance trabecular patterns on dental radiographs towards detecting fractures. Manoj *et al.* [19] propose a mechanism to enhance dental radiographs corrupted by quantum noise.

1.3. LACUNA OF REVIEW AND GAPS

Despite the wide popularity and applications of Unsharp Masking, it has serious limitations also. Clark *et al.* [20] have demonstrated that Unsharp Masking enhances the perceptual quality of dental radiographs and it produces overshoot artefact and amplifies noise that will adversely influence the accuracy of diagnosis. The overshoot artefact may be misinterpreted as a prosthesis misfit or pathosis. Brettle and Carmichael [21] also demonstrated that the artefacts caused by image processing, particularly at high contrast boundaries, closely mimic the pathological features associated with restorations and invite the risk of unwanted interventions.

1.4. CONTRIBUTIONS, NOVELTY, AND HIGHLIGHTS

Contributions: To resolve the issues of noise-amplification, overshoot artefact, haloes, and discontinuity artefact in the Unsharp Masking, a novel algorithm, termed Gradient-adaptive Nonlinear Sharpening (GNS), for improving the acuity of edges in the dental radiographs, is introduced in this paper.

Novelty: In the conventional Unsharp Masking algorithm, the product of the arbitrary scalar termed as 'scale' and the difference between the input image and its Gaussian smoothed version, after a thresholding process is added back to the input image itself. The Gaussian smoothing kernel used in the Unsharp Masking is a linear filter. The weights in the kernel depend only on the spatial distance from the center. The Gaussian kernel has the same smoothing response on noise-affected pixels and edges. Hence, it cannot be expected that the difference between the input image and its Gaussian smoothed version may have higher values at the edge pixels compared to the noise-affected pixels. It is difficult to distinguish the noise-affected pixels and the edge pixels from the difference between the input image and its Gaussian smoothed version, via the thresholding operation. In GNS, the Gaussian kernel is replaced by the Adaptive Edge Smoothing Filter (AESF). AESF is a locally-adaptive 2D Gaussian smoothing kernel whose variance is directly proportional to the local value of the gradient magnitude. It smooths the edge pixels more strongly than the noise-affected pixels. Consequently, the difference between the input image and output of AESF will be significantly high at the edge pixels compared to the noise-affected pixels. The concept of the Adaptive Edge Smoothing Filter is new in image processing itself. Readers should not be confused with the edge-preserving filters. The operation of the adaptive edge smoothing filter is just opposite to that of the edge-preserving filters.

The thresholding process in the Unsharp Masking is a mathematical function with jump discontinuity. Because of the thresholding process, Unsharp Masking is prone to discontinuity artefact. Instead of the thresholding process in the Unsharp Masking, in GNS, the difference between the output of the AESF and the input image is weighted by the normalized gradient magnitude. This nonlinear weighting is a continuous function and avoids the issue of discontinuity artefact. As the thresholding process is not used in GNS, it is free from the burden of tuning the 'threshold' parameter. GNS has less number of operational parameters compared to the Unsharp Masking.

Highlights: (i) Because of the characteristics of AESF used in GNS and the nonlinear weighting process involved in its computation, it is free from noise-amplification and overshoot artefact. (ii) As no mathematical operation with jump discontinuity is involved in the GNS, it is free from the discontinuity artefact. (iii) GNS has less number of operational parameters compared to Unsharp Masking.

2. METHODS

2.1 GRADIENT-ADAPTIVE NONLINEAR SHARPENING (GNS)

In GNS, the product of the arbitrary scalar termed as 'scale' and the difference between the output of the Adaptive Edge Smoothing Filter (AESF) and the input image, weighted by the normalized gradient

magnitude is added to the input image. AESF is a locally-adaptive 2D Gaussian smoothing kernel whose standard deviation is directly proportional to the local value of the gradient magnitude. The first step in GNS is to compute the normalized gradient. The gradient magnitude is computed from the gradients along the rows (horizontal direction) and the columns (vertical direction) of the input radiograph.

$$G = \sqrt{(G_r)^2 + (G_c)^2} \quad (1)$$

In (1), G_r is the gradient along rows (horizontal direction), and G_c is the gradient along columns (vertical direction). G is the 2D vector comprising local values of the gradient magnitude. The gradient along rows and gradient along columns are computed by convolving the input radiograph, with respective Sobel convolution masks.

$$G_r = f ** S_r \text{ and } G_c = f ** S_c \quad (2)$$

In (2), f is the input radiograph. The notion, $**$ indicates 2D convolution. S_r and S_c respectively are Sobel masks along rows and columns.

$$S_r = \begin{bmatrix} +1 & 0 & -1 \\ +2 & 0 & -2 \\ +1 & 0 & -1 \end{bmatrix} \text{ and } S_c = \begin{bmatrix} +1 & +2 & +1 \\ 0 & 0 & 0 \\ -1 & -2 & -1 \end{bmatrix} \quad (3)$$

The 2D gradient vector is normalised with the maximum value in it. The normalisation yields,

$$g = \frac{G}{G_{max}} \quad (4)$$

In (4), g is the normalized 2D gradient vector. G_{max} is the largest gradient value. In GNS, the Gaussian kernel in the Unsharp Masking is replaced by the Adaptive Edge Smoothing Filter. As pointed out, AESF is a locally-adaptive 2D Gaussian smoothing kernel whose variance is directly proportional to the local value of the gradient magnitude. It smooths the edge pixels more strongly than the noise-affected pixels. Consequently, the difference between the input image and output of AESF will be significantly high at the edge pixels compared to the noise-affected pixels. The output of the AESF at a pixel location (r,c) ,

$$\tilde{f}(r,c) = \sum_{p=-w}^{+w} \sum_{q=-w}^{+w} K(p,q)f(r+p,c+q), \quad 1 \leq r \leq R \text{ and } 1 \leq c \leq C \quad (5)$$

In (5), R and C are the number of rows and the number of columns in the input radiograph. K is the adaptive edge-smoothing Gaussian kernel. w is the radius of the adaptive Gaussian kernel. The kernel at a pixel location (r,c) is,

$$K_{rc}(p,q) = \frac{1}{2\pi(\sigma_{rc})^2} e^{-\left(\frac{p^2+q^2}{2(\sigma_{rc})^2}\right)}, \quad -w \leq p \leq +w \text{ and } -w \leq q \leq +w \quad (6)$$

In (6), σ_{rc} is the local value of the standard deviation of the adaptive Gaussian kernel. The local value of the standard deviation of the adaptive Gaussian kernel is the product of the corresponding value in the nor-

malised gradient vector and the maximum limit of the standard deviation of the adaptive Gaussian kernel. It is computed as,

$$\sigma_{rc} = \sigma_{max}[g(r,c)] \quad (7)$$

In (7), σ_{max} is the maximum limit of the standard deviation of the adaptive Gaussian kernel. It has to be as high as possible. Its value is kept as 100 in this paper. The radius of the kernel, w , also needs to be high. The radius of the adaptive Gaussian kernel is set as 9×9 , in this paper. The adaptive Gaussian kernel is normalised such that,

$$K_{rc}(p,q) = \frac{K_{rc}(p,q)}{\sum_{p=-w}^{+w} \sum_{q=-w}^{+w} K_{rc}(p,q)} \quad (8)$$

The difference between the input image and output of the Adaptive Edge Smoothing Filter,

$$d = f - \tilde{f} \quad (9)$$

The thresholding process in the Unsharp Masking is a mathematical function with jump discontinuity. Because of the thresholding process, Unsharp Masking is prone to discontinuity artefact. Instead of the thresholding process in the Unsharp Masking, in GNS, the difference between the output of the AESF and the input image is weighted by the normalised gradient magnitude. This nonlinear weighting is a continuous function and avoids the issue of discontinuity artefact. As the thresholding process is not used in GNS, it is free from the burden of tuning the 'threshold' parameter. As mentioned, each value in the 2D vector corresponding to the difference, d is weighted by the corresponding value in the normalized gradient vector as,

$$e = \Gamma(d,g) \quad (10)$$

The operator, Γ in (9) indicates element-wise multiplication. The sharpened radiograph,

$$\hat{f} = f + \alpha e \quad (11)$$

In (10), α is an arbitrary parameter that determines the strength of sharpening. This parameter is called as the scale. The Schematic of the steps involved in the computation of the sharpened image in GNS described in (1) to (10) is shown in Fig. 1.

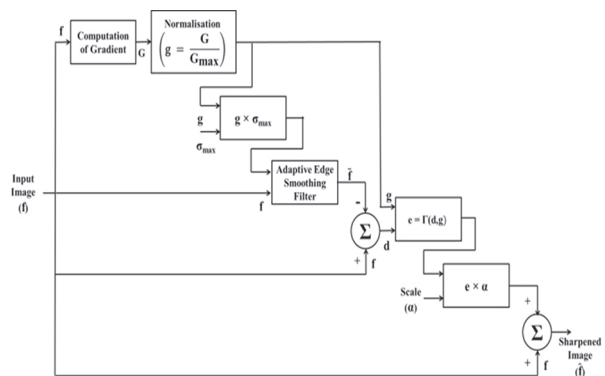


Fig. 1. Schematic of the steps involved in the computation of the sharpened image in GNS

2.2. TEST IMAGES

The dataset used in this paper is downloaded from the Mendeley data repository [22]. This is the data associated with Abdi *et al.* [23] and the dataset comprises of annotated panoramic dental radiographs of 116 patients. All images are in .png format. The images are taken by using the Soredex CranexD digital panoramic x-ray unit available at Noor Medical Imaging Centre, Qom, Iran. The subjects cover a wide range of dental conditions from healthy, to partial and complete edentulous cases.

2.3. PROTOCOL FOR PARAMETER SELECTION AND PERFORMANCE EVALUATION

Sharpening is helpful to improve the acuity of edges. However, most of the sharpening algorithms produce inadvertent artefacts like contrast overshoot, edge-widening or haloes, and noise amplification. There are no unique image quality metrics that can reflect the overall quality of the sharpened images accounting for all these quality aspects and artefacts. Hence, the performance evaluation of the sharpening techniques is a non-trivial task.

Krasula *et al.* [24] have recently proposed a framework governing the subjective evaluation of the quality of the sharpened images and have suggested certain objective measures which can be used for the quantitative performance assessment of the sharpening schemes. As an addition to the framework for evaluating the performance of the sharpening algorithms on natural-scene images reported in [24], J. Joseph and R. Periyasamy [25] have suggested four quality metrics particularly useful for evaluating the performance of sharpening algorithms on medical images. They are the Saturation Evaluation Index (SEI) [26], Sharpness of Ridges (SOR) [27], Edge Model-Based Contrast Measure (EMBCM) [28], and Visual Information Fidelity (VIF) [29]. These four quality statistics are used in this paper to aid the selection of the scale value in GNS and for comparing the performance of GNS with the Unsharp Masking.

The SEI reflects the quality degradation in terms of intensity saturation caused by the contrast overshoot. The value of SEI is expected to be as low as possible, ideally 0. SOR is a metric that quantitatively shows how far the quality of edges in the sharpened images is degraded by amplified noise content. Like SEI, the value of SOR is also supposed to be as low as possible. A good sharpening, free from haloes is always expected to produce thin and sharp edges. While assessing the quality of edges, their width also needs to be taken into account. The EMBCM is the only sharpness metric that considers the width of the edges as well. EMBCM is an unbounded statistic whose value is expected to be as high as possible. VIF accounts for the overall information fidelity in the sharpened images concerning that in the input image. Like EMBCM, the value of VIF will be high if the sharpening produces artefact-free (free from

overshoot, noise-amplification, haloes, and discontinuity artefact) output images with thin and sharp edges.

2.4. SYSTEM REQUIREMENTS

All experiments are conducted with Matlab® software. The version of the software is 7.12.0.635 (R2018a) with License Number: 161052. The software is installed in a desktop computer with Intel (R), Pentium (R) Processor, and CPU B950 @ 2.10 GHz. The installed Memory (RAM) is 4 GB. Operating System is Microsoft Windows 7 Version 6.1 (Build 7601: Service Pack 1), 64-bit.

3. RESULTS

The influence of the selection of the scale value in GNS on the subjective quality of the sharpened images and the objective quality measures like SEI, SOR, EMBCM, and VIF is discussed in this section. Out of the total 116 radiographs, three test images for which the pictorial results are presented are shown in Fig. 2.

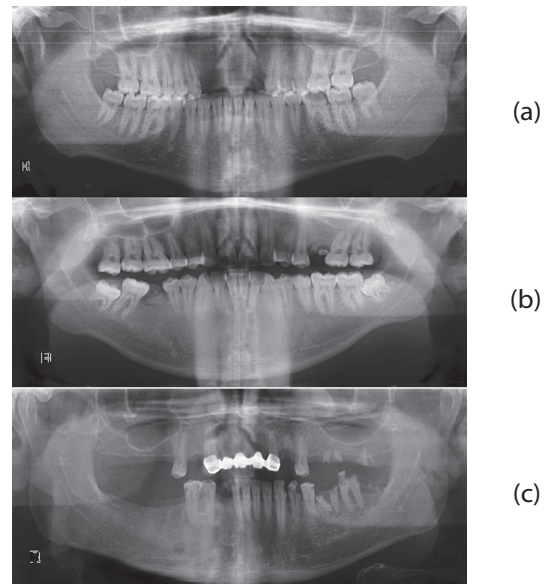


Fig. 2. Test images (a) Test image 1 (b) Test image 2 (c) Test image 3

Enlarged portions of the output images of GNS corresponding to the input image 1, input image 2 and input image 3 for various scale values are shown in Fig. 3 to Fig. 5. When the scale is equal to 1, (Fig. 3 (b), Fig. 4 (b) and Fig. 5 (b)) significant improvement in edge strength is not evident. When the scale value increases from 1 to 4, (Fig. 3 (c) to Fig. 3 (d), 4 (c) to Fig. 4 (d) and 5 (c) to Fig. 5 (d)), the strength of edges increases to a clearly visible level. When the scale value is greater than 5, (Fig. 3 (f) to Fig. 3 (i), 4 (f) to Fig. 4 (i) and 5 (f) to Fig. 5 (i)), the noise content gets amplified slightly. However, the amplification of noise is not as critical as in the Unsharp Masking. The value of the scale in GNS is within the range of 3 to 5, the strength of edges in the dental radiographs gets enhanced to a visibly apparent level without amplifying the noise significantly. The observation is found to be consistent on all 116 test images.

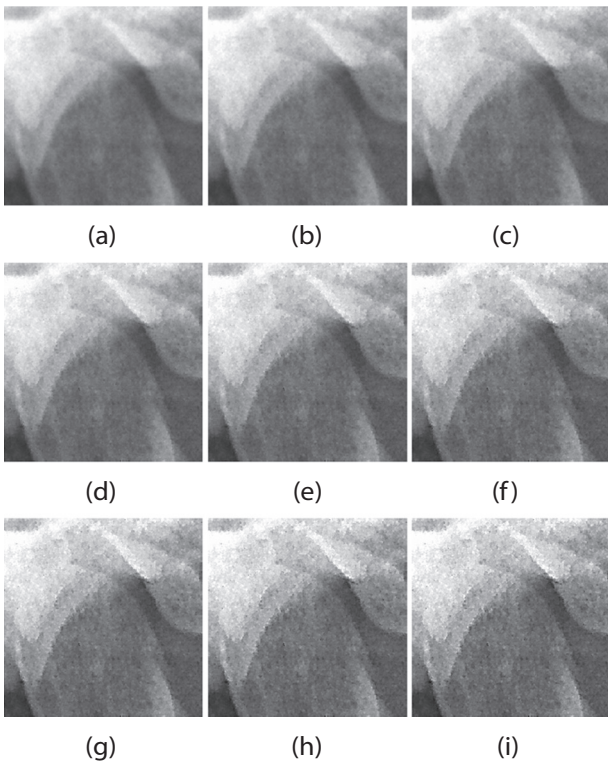


Fig. 3. Enlarged portions of the output images of GNS corresponding to the input image 1 for various scale values (a) Enlarged portion of the input image 1 (b) Scale = 1 (c) Scale = 2 (d) Scale = 3 (e) Scale = 4 (f) Scale = 5 (g) Scale = 6 (h) Scale = 7 (i) Scale = 8

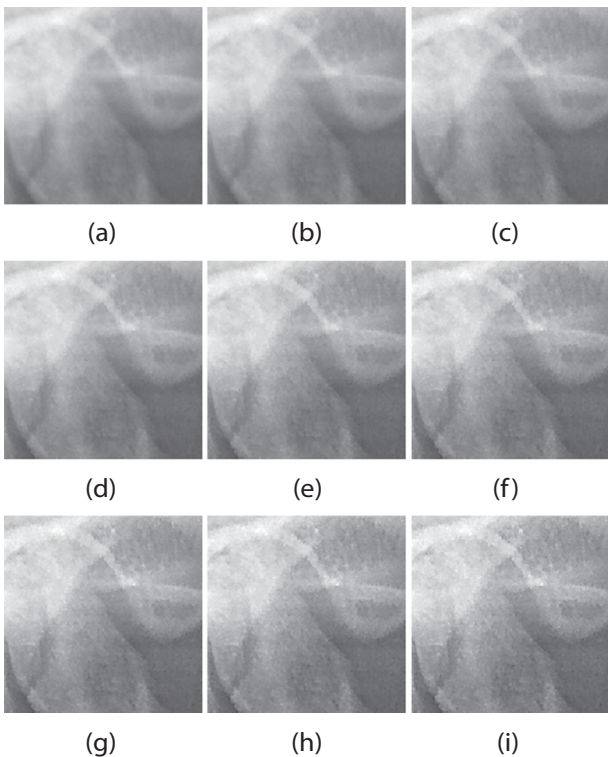


Fig. 4. Enlarged portions of the output images of GNS corresponding to the input image 2 for various scale values (a) Enlarged portion of the input image 2 (b) Scale = 1 (c) Scale = 2 (d) Scale = 3 (e) Scale = 4 (f) Scale = 5 (g) Scale = 6 (h) Scale = 7 (i) Scale = 8

Influence of the scale value on SEI, SOR, EMBCM and VIF is illustrated in Fig. 6. The variations of the SEI with scale for three test radiographs are shown in Fig. 6 (a). The slopes of the SEI versus scale curves for all three test images are very low as seen in Fig. 6 (a). SEI does not increase critically in response to the increase in the value of scale. Even at high values of the scale, the increase in SEI is not significant. This is a clear indication that GNS produces sharpened images free from intensity saturation. The variations of the SOR with scale for three test radiographs are shown in Fig. 6 (b). Similar to the SEI versus scale curves, slopes of the SOR versus scale curves for all three test images are very low as seen in Fig. 6 (b). SOR does not increase critically, in response to the increase in the value of scale. Even at high values of the scale, the increase in SOR is not significant. This is a clear indication that even at high values of the scale, quality of the edges in the output images produced by the GNS is not significantly affected by the amplified noise content.

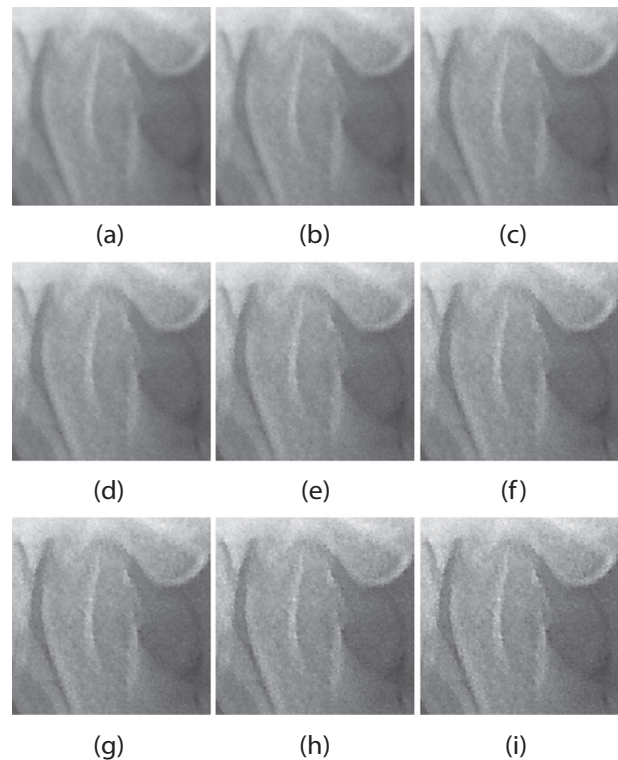
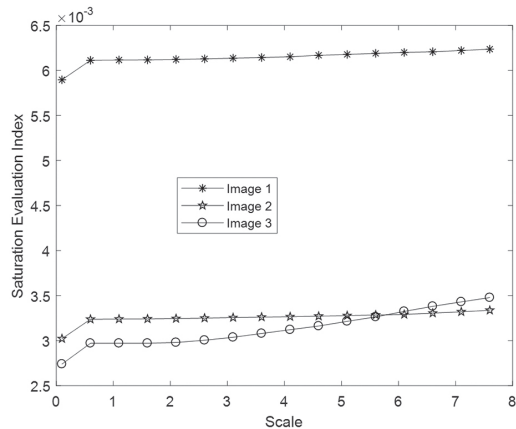


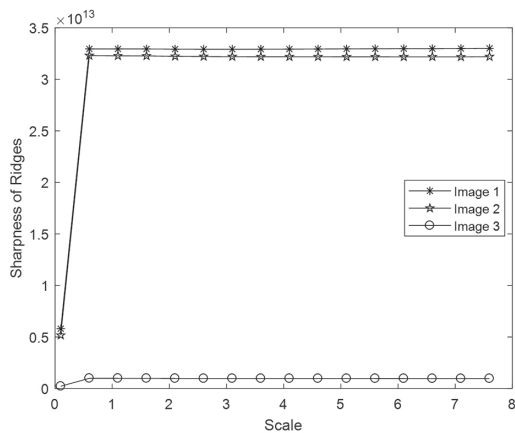
Fig. 5. Enlarged portions of the output images of GNS corresponding to the input image 3 for various scale values (a) Enlarged portion of the input image 3 (b) Scale = 1 (c) Scale = 2 (d) Scale = 3 (e) Scale = 4 (f) Scale = 5 (g) Scale = 6 (h) Scale = 7 (i) Scale = 8

In the EMBCM versus scale curves in Fig. 6 (c), the slopes of the curves are relatively higher when the value of the scale is less than 4 compared to the slopes of the curves when the scale is above 4. As mentioned already, the EMBCM reflects the quality of the edges in terms of their sharpness and thinness. From the EMBCM versus scale curves, it can be inferred that GNS offers relatively better output images comprising sharper

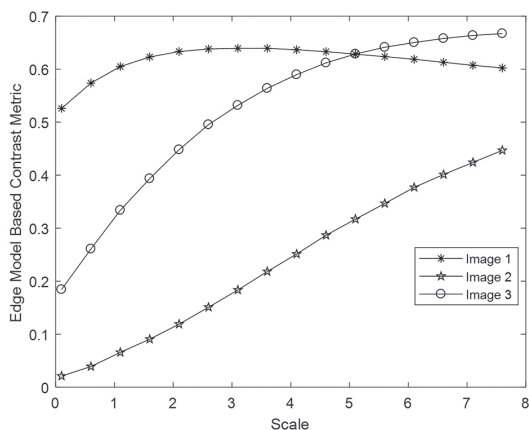
and thinner edges when the scale value is less than 4. In the VIF versus scale curves in Fig. 6 (d), VIF is at its maximum for the input image 1, when the scale value is equal to 3. For input image 2 and input image 3, the maximum values of VIF are observed at the scale values equal to 3.5 and 6.5, respectively. As per the observations drawn out from the VIF versus scale curves of 116 test radiographs, the VIF is found to be at its maximum for a range of scale values between 3 and 7. From the variations of the SEI, SOR, EMBCM, and VIF against the scale values, the practically efficient range of scale suitable for dental radiographs can be considered as between 4 and 5.



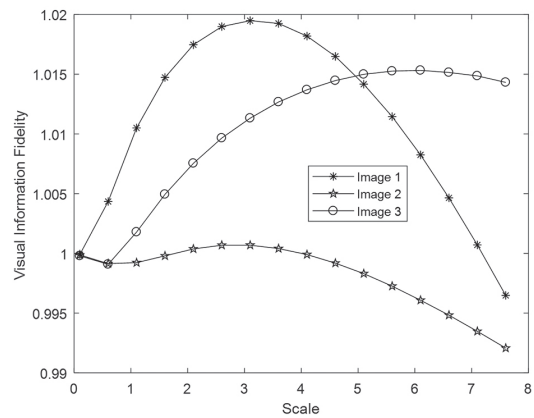
(a)



(b)



(c)



(c)

Fig. 6. Influence of the scale value on various objective image quality measures (a) SEI versus scale (b) SOR versus scale (c) EMBCM versus scale (d) VIF versus scale

4. DISCUSSIONS

In this section, the performance of the GNS is compared with the Unsharp Masking in terms of quality of the sharpened images and the values of the objective quality measures. Enlarged portions of the output images of the Unsharp Masking and GNS for three test radiographs are shown in Fig. 7 to Fig. 9.

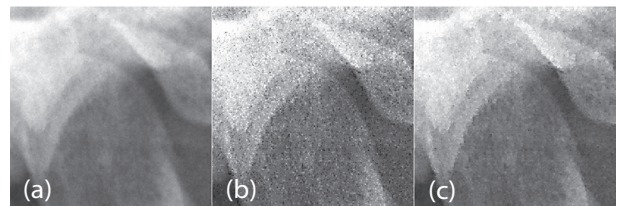


Fig. 7. Sharpened images (a) Enlarged portion of the input image 1 (b) Enlarged portion of the output of Unsharp Masking (c) Enlarged portion of the output of GNS

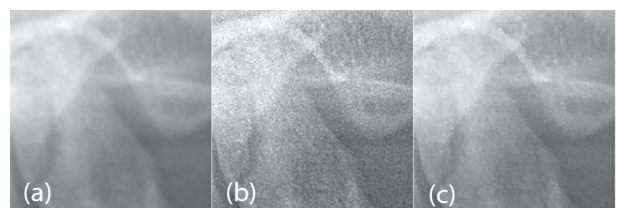


Fig. 8. Sharpened images (a) Enlarged portion of the input image 2 (b) Enlarged portion of the output of Unsharp Masking (c) Enlarged portion of the output of GNS

In both the Unsharp Masking and the GNS, the value of scale is set as equal to 5. The threshold in the Unsharp Masking is set equal to 0.1. It can be seen in the output images of the Unsharp Masking furnished in Fig. 7 (b), Fig. 8 (b) and Fig. 9 (b) that noise content is significantly amplified. It is evident in Fig. 7 (c), Fig. 8 (c) and Fig. 9 (c), GNS produces output images in which the edges are

sharper than those in the input images furnished in 7 (a), Fig. 8 (a) and Fig. 9 (a). Amplification of the noise content in GNS is not as critical as in the Unsharp Masking.

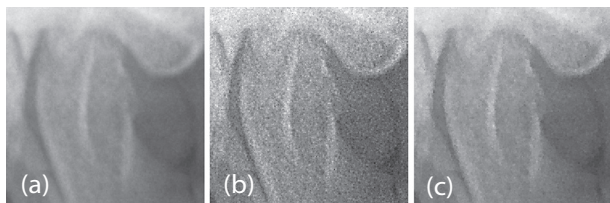


Fig. 9. Sharpened images (a) Enlarged portion of the input image 3 (b) Enlarged portion of the output of Unsharp Masking (c) Enlarged portion of the output of GNS

Values of SEI, SOR, EMBCM and VIF shown by the Unsharp Masking and GNS, corresponding to the output images furnished in Fig. 7 to Fig. 9 are shown in table 1 and table 2, respectively. The summary of these quality metrics on 116 test radiographs is furnished in table 3. GNS exhibited lower values of SEI and SOR and higher values of EMBCM and VIF, compared to the Unsharp Masking. Lower values of SEI and SOR, respectively indicate that GNS is free from overshoot artefact and saturation and the quality of edges in the output images of GNS is less affected by noise. Higher values of EMBCM and VIF, respectively confirm that GNS is free from haloes as it produces thin and sharp edges and the sharpened images are of good information fidelity.

Table 1. Values of quality metrics shown by the Unsharp Masking

Quality Metric	Image 1	Image 2	Image 3
SEI	0.0072	0.0036	0.0035
SOR	7.3205×10^{13}	5.7376×10^{13}	1.4223×10^{12}
EMBCM	0.5604	0.0227	0.2070
VIF	0.9757	0.9979	0.9957
Computational Time (S)	0.37	0.29	0.19

Table 2. Values of quality metrics shown by the GNS

Quality Metric	Image 1	Image 2	Image 3
SEI	0.0062	0.0033	0.0032
SOR	3.2948×10^{13}	3.2183×10^{13}	9.7641×10^{11}
EMBCM	0.6297	0.3117	0.6259
VIF	1.0147	0.9985	1.0149
Computational Time (S)	1626.05	1773.22	1595.04

Table 3. Summary of quality metrics shown by the Unsharp Masking and GNS on 116 images

Quality Metric	Unsharp Masking	GNS
SEI	0.0048 ± 0.0021	0.0042 ± 0.0017
SOR	$4.4 \times 10^{13} \pm 3.8 \times 10^{13}$	$2.2 \times 10^{13} \pm 1.8 \times 10^{13}$
EMBCM	0.2634 ± 0.2732	0.5224 ± 0.1825
VIF	0.9898 ± 0.0122	1.0094 ± 0.0094
Computational Time (S)	0.2833 ± 0.0902	1664.8 ± 95.19

Table 4. Comparison of the proposed model with other state of art architectures using Unsharp Masking mechanisms, without considering the tolerance range

Methods	SEI	SOR	EMBCM	VIF
Manoj et al. [19]	0.0044	3.7×10^{13}	0.4178	0.8990
Clark et al. [20]	0.0098	5.7×10^{13}	0.2065	0.8956
Geraets et al. [18]	0.0048	4.4×10^{13}	0.2634	0.9898
Proposed Model	0.0042	2.2×10^{13}	0.5224	1.0094

It is believed that noise-amplification in the Unsharp Masking can be reduced by increasing the value of the threshold. But increasing the value of the threshold may introduce discontinuity artefact. Enlarged portions of the output images of the Unsharp Masking corresponding to the three test images for a threshold value equal to 0.5 and scale equal to 5 are shown in Fig. 10. Black and white spots are visible on the output images of the Unsharp Masking. These spots are caused by the discontinuity artefact. As no thresholding process is involved in GNS, the output images produced by GNS are free from the discontinuity artefact.

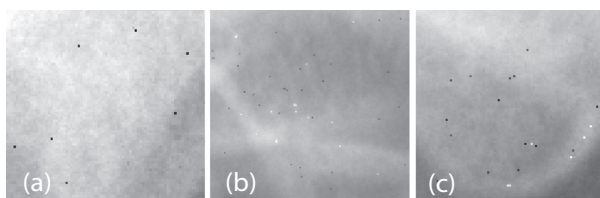


Fig. 10. Discontinuity artefact in the Unsharp Masking (a) Enlarged portion of input image 1 sharpened by the Unsharp Masking (b) Enlarged portion of input image 2 sharpened by the Unsharp Masking (c) Enlarged portion of input image 3 sharpened by the Unsharp Masking

To evaluate the efficacy of the proposed model, the scores of the quality metrics namely SEI, SOR, EMBCM, and VIF are compared to other architectures employed for dental radiograph enhancements. The methods have been evaluated on the Mendeleev data repository [18]. The finding is illustrated in Table 4. It can be observed that the proposed model outperforms the competitors in all the metrics. One downside of the proposed model is that its computational time required is on the higher scale compared to its competitors.

5. CONCLUSION AND FUTURE SCOPE

5.1. CONCLUSION

Summary of Contributions: A noise-robust and overshoot-free alternative to the Unsharp Masking, called Gradient-adaptive Nonlinear Sharpening (GNS), for enhancing the quality of edges in dental radiographs was proposed in this paper.

Summary of Observations: GNS exhibited lower values of SEI and SOR and higher values of EMBCM and

VIF, compared to the Unsharp Masking. Lower values of SEI and SOR, respectively indicate that GNS is free from overshoot artefact and saturation and the quality of edges in the output images of GNS is less affected by noise. Higher values of EMBCM and VIF, respectively confirm that GNS is free from haloes as it produces thin and sharp edges and the sharpened images are of good information fidelity.

Advantages of GNS: Unlike the conventional Unsharp Masking, the computation of sharpened images in the proposed GNS does not involve any thresholding operation. Hence GNS is free from discontinuity artefact. GNS has less number of operational parameters compared to the Unsharp Masking. Because of the Adaptive Edge Smoothing Filter (AESF) and local gradient-based weighting of the difference image in LGUM, it is free from noise-amplification and sharpness overshoot. GNS selectively sharpen the edges without amplifying the noise content.

Applications / Commercial Viability of GNS: GNS can be used as a pre-processing algorithm in image processing tools used in clinical practice and forensic odontology for the automated analysis of dental radiographs. It helps to improve the efficiency of segmentation algorithms used in such image processing tools.

5.2. LIMITATIONS OF GNS AND FUTURE SCOPE

The GNS has three operational parameters. They are the radius of the AESF, maximum limit of the standard deviation of AESF and scale. Adaptive methods for identifying the optimum value of these operational parameters will help to eliminate the burden of tuning them. The GNS is computationally intense compared to the conventional Unsharp Masking, because of the local processing strategy adopted in it. Methods which can accelerate the computation of GNS will make it more advantageous.

6. REFERENCES:

- [1] J. Krois et al. "Deep learning for the radiographic detection of periodontal bone loss", Scientific reports, Vol. 9. No. 1, 2019, p.8495.
- [2] J. Kim, H. Lee, I. Song, "DeNTNet: Deep Neural Transfer Network for the detection of periodontal bone loss using panoramic dental radiographs", Nature Scientific Reports, Vol. 9, No. 1, 2019, p. 17615.
- [3] M.A. Alzubaidi, M. Otoom, "A comprehensive study on feature types for osteoporosis classification in dental panoramic radiographs", Computer Methods and Programs in Biomedicine, Vol. 188, 2020, p. 105301.
- [4] I. Aliaga, V. Vera, M. Vera, E. García, M. Pedrera, G. Pajares, "Automatic computation of mandibular indices in dental panoramic radiographs for early osteoporosis detection", Artificial Intelligence in Medicine, Vol. 103, 2020, p. 101816.
- [5] S. Javed, M. Zakirulla, R. U. Baig, S. M. Asif, A. B. Meer, "Development of artificial neural network model for prediction of post-streptococcus mutans in dental caries", Computer Methods and Programs in Biomedicine, Vol. 186, 2020, p. 105198.
- [6] A. Heinrich, F. V. Güttler, S. Schenkl, "Automatic human identification based on dental X-ray radiographs using computer vision", Nature Scientific Reports, Vol. 10, No. 1, 2020, p. 3801.
- [7] H. Chen, K. Zhang, P. Lyu, "A deep learning approach to automatic teeth detection and numbering based on object detection in dental periapical films", Nature Scientific Reports, Vol. 9, No. 1, 2019, pp. 1-11.
- [8] S. Vinayahalingam, T. Xi, S. Bergé, "Automated detection of third molars and mandibular nerve by deep learning", Nature Scientific Reports, Vol. 9, No. 1, 2019, p. 9007.
- [9] T. E. Southard, K. A. Southard, "Performance of filters for noise reduction in maxillary alveolar bone imaging", IEEE Transactions on Biomedical Engineering, Vol. 42, No. 1, 1995, pp. 13-20.
- [10] I. Frosio, C. Olivieri, M. Lucchese, N. A. Borghese, P. Boccacci, "Bayesian denoising in digital radiography: A comparison in the dental field", Computerized Medical Imaging and Graphics, Vol. 37, No. 1, 2013, pp. 28-39.
- [11] H. Rahmi-Fajrin, S. Puspita, S. Riyadi and E. Sofiani, "Dental radiography image enhancement for treatment evaluation through digital image processing", Journal of Clinical and Experimental Dentistry, Vol. 10, No. 7, 2018, pp. 629-634.
- [12] I. Draganov, V. Gancheva. "Unsharp Masking with Local Adaptive Contrast Enhancement of Medical Images", Proceedings of International Conference on Medical Imaging and Computer-Aided Diagnosis Medical Imaging and Computer-Aided Diagnosis, Lecture Notes in Electrical Engineering, Springer, Singapore, Vol. 784, 2021, pp. 354-363.
- [13] Y. Yan et al. "Bi-SCM: bidirectional spiking cortical model with adaptive unsharp masking for mam-

- mography image enhancement”, *Multimedia Tools and Applications*, Vol. 82, No. 8, 2023, pp. 12081-12098.
- [14] A. Kumar, P. Kumar, S. Srivastava, “A skewness reformed complex diffusion based unsharp masking for the restoration and enhancement of Poisson noise corrupted mammograms”, *Biomedical Signal Processing and Control*, Vol. 73, 2022, p. 103421.
- [15] M. Fujita, Y. Kodera, M. Ogawa, K. Tanimoto, T. Sunayashiki, T. Wada, K. Doi, “Digital image processing of dento-maxillofacial radiographs”, *Oral Surgery, Oral Medicine, Oral Pathology*, Vol. 64, No. 4, 1987, pp. 485-493.
- [16] T. Harada, K. Nishikawa, K. Kuroyanagi, “Unsharp masking technique as a pre-processing filter for improvement of 3D-CT image of bony structure in the maxillofacial region”, *Oral Radiology*, Vol. 14, 1998, pp. 85-94.
- [17] R. A. Couture, B. R. Whiting, C. F. Hildebolt, D. A. Dixon, “Visibility of trabecular structures in oral radiographs”, *Oral Surgery, Oral Medicine, Oral Pathology, Oral Radiology and Endodontology*, Vol. 96, No. 6, 2003, pp. 764-771.
- [18] W. Geraets, G. Jonasson, M. Hakeberg, “Predicting fractures using trabecular patterns on panoramic radiographs”, *Clinical Oral Investigations*, Vol. 22, No. 1, 2018, pp. 377-384.
- [19] M. T. Joy, B. P. Shan, G. Titus, “Restoration of dental radiographs corrupted by quantum noise via a noise-adaptive sub-global weighted sum of radiometrically similar pixels”, *International Journal of Computational Biology and Drug Design*, Vol. 15, No. 3, 2023, pp. 249-266.
- [20] J. L. Clark, C. P. Wadhvani, K. Abramovitch, D. D. Rice, M. T. Kattadiyil, “Effect of image sharpening on radiographic image quality”, *The Journal of Prosthetic Dentistry*, Vol. 120, No. 6, 2018, pp. 927-933.
- [21] D. Brettle, F. Carmichael, “The impact of digital image processing artefacts mimicking pathological features associated with restorations”, *British Dental Journal*, Vol. 211, No. 4, 2011, pp. 167-170.
- [22] A. H. Abdi, S. Kasaei, “Panoramic Dental X-rays with Segmented Mandibles”, *Mendeley Data*, V1, 2017, <http://dx.doi.org/10.17632/hxt48yk462.1>.
- [23] A. H. Abdi, S. Kasaei, M. Mehdizadeh, “Automatic segmentation of mandible in panoramic x-ray”, *Journal of Medical Imaging*, Vol. 2, No. 4, 2015, p. 44003.
- [24] L. Krasula, P. Le Callet, K. Fliegel, M. Klíma, “Quality Assessment of Sharpened Images: Challenges, Methodology, and Objective Metrics”, *IEEE Transactions on Image Processing*, Vol. 26, No. 3, 2017, pp. 1496-1508.
- [25] J. Joseph, R. Periyasamy, “Nonlinear sharpening of MR images using a locally adaptive sharpness gain and a noise reduction parameter”, *Pattern Analysis and Applications*, Vol. 22, No. 1, 2019, pp. 273-283.
- [26] J. Joseph, R. Periyasamy, “A fully customized enhancement scheme for controlling brightness error and contrast in magnetic resonance images”, *Biomedical Signal Processing and Control*, Vol. 39, 2018, pp. 271-283.
- [27] V. S. Hari, V. P. J. Raj, R. Gopikakumari, “Unsharp masking using quadratic filter for the enhancement of fingerprints in noisy background”, *Pattern Recognition*, Vol. 46, No. 12, 2013, pp. 3198-3207.
- [28] J. Guan, W. Zhang, J. Gu, H. Ren, “No-reference blur assessment based on edge modelling”, *Journal of Visual Communication and Image Representation*, Vol. 29, 2015, pp. 1-7.
- [29] H. R. Sheikh, A. C. Bovik, G. de Veciana, “An information fidelity criterion for image quality assessment using natural scene statistics”, *IEEE Transactions on Image Processing*, Vol. 14, No. 12, 2005, pp. 2117-2128.